5. A. Lanzara *et al.*, *Nature* **412**, 510 (2001).
6. T. P. Devereaux, T. Cuk, Z.-X. Shen, N. Nagaosa, *Phys. Rev. Lett.* **93**, 117004 (2004).
7. T. Dahm *et al.*, *Nat. Phys.* **5**, 217 (2009).
8. D. Reznik *et al.*, *Nature* **440**, 1170 (2006).
9. M. Le Tacon *et al.*, *Nat. Phys.* **7**, 725 (2011).
10. Y. Li *et al.*, *Nature* **468**, 283 (2010).
11. J. Lee *et al.*, *Nature* **442**, 546 (2006).
12. O. Ahmadi, L. Coffey, J. F. Zasadzinski, N. Miyakawa, L. Ozyuzer, *Phys. Rev. Lett.* **106**, 167005 (2011).
13. M. Norman, A. Chubukov, *Phys. Rev. B* **73**, 140501 (2006).
14. J. Hwang, T. Timusk, E. Schachinger, J. Carbotte, *Phys. Rev. B* **75**, 144508 (2007).
15. E. van Heumen *et al.*, *Phys. Rev. B* **79**, 184512 (2009).
16. L. Perfetti *et al.*, *Phys. Rev. Lett.* **99**, 197001 (2007).
17. F. Carbone, D.-S. Yang, E. Giannini, A. H. Zewail, *Proc. Natl. Acad. Sci. U.S.A.* **105**, 20161 (2008).
18. See supporting material on *Science* Online.
19. C. Giannetti *et al.*, *Nat. Commun.* **2**, 353 (2011).
20. H. Eisaki *et al.*, *Phys. Rev. B* **69**, 064512 (2004).
21. D. van der Marel *et al.*, *Nature* **425**, 271 (2003).
22. S. Johnston *et al.*, http://arxiv.org/pdf/1101.1302.pdf (2011).
23. N. Kovaleva *et al.*, *Phys. Rev. B* **69**, 054511 (2004).
24. H. J. Kaufmann, E. G. Maksimov, E. K. H. Salje, *J. Superconduct.* **22**, 755 (1998).
25. F. Cilento *et al.*, *Appl. Phys. Lett.* **96**, 021102 (2010).
26. P. B. Allen, *Phys. Rev. Lett.* **59**, 1460 (1987).
27. P. B. Allen, R. Dynes, *Phys. Rev. B* **12**, 905 (1975).
28. A. J. Millis, S. Sachdev, C. M. Varma, *Phys. Rev. B* **37**, 4975 (1988).
29. C. Gadermaier *et al.*, *Phys. Rev. Lett.* **105**, 257001 (2010).
30. A. S. Mishchenko, N. Nagaosa, *Phys. Rev. Lett.* **93**, 036402 (2004).
31. G. Sangiovanni, O. Gunnarsson, E. Koch, C. Castellani, M. Capone, *Phys. Rev. Lett.* **97**, 046404 (2006).
32. H. Iwasawa *et al.*, *Phys. Rev. Lett.* **101**, 157005 (2008).
33. E. Schachinger, J. Carbotte, T. Timusk, *Europhys. Lett.* **86**, 67003 (2009).

Acknowledgments: We thank M. Capone and A. Chubukov for discussions and suggestions. Partially supported by the Università Cattolica del Sacro Cuore (grant D2.2 2010) (C.G., F.B., and G.F.), by the Italian Ministry of University and Research (grants FIRBRBAP045JF2 and FIRB-RBAP06AWK3) (F.C., G.C., and F.P.) and by the Swiss National Science Foundation (grant 200020-130052) and its Materials with Novel Electronic Properties (MaNEP) program (D.v.d.M.). The crystal growth work was performed in M.G.'s prior laboratory at Stanford University, supported by the U.S. Department of Energy under contract DE-AC03-76SF00515. Work at the University of British Columbia was supported by the Killam, Sloan Foundation, and Canada Research Chair Programs, the Steacie Fellowship Program of the Natural Sciences and Engineering Research Council of Canada (NSERC), the Canada Foundation for Innovation (CFI), NSERC, the Canadian Institute for Advanced Research (CIFAR) Quantum Materials Program, and the British Columbia Synchrotron Institute (BCSI).

Supporting Online Material

www.sciencemag.org/cgi/content/full/335/6076/1600/DC1
Materials and Methods
Fig. S1
Table S1
References (*34*, *35*)

17 November 2011; accepted 24 February 2012
10.1126/science.1216765

Coherent Sensing of a Mechanical Resonator with a Single-Spin Qubit

Shimon Kolkowitz,[1]* Ania C. Bleszynski Jayich,[2]* Quirin P. Unterreithmeier,[1]* Steven D. Bennett,[1] Peter Rabl,[3] J. G. E. Harris,[4] Mikhail D. Lukin[1]†

Mechanical systems can be influenced by a wide variety of small forces, ranging from gravitational to optical, electrical, and magnetic. When mechanical resonators are scaled down to nanometer-scale dimensions, these forces can be harnessed to enable coupling to individual quantum systems. We demonstrate that the coherent evolution of a single electronic spin associated with a nitrogen vacancy center in diamond can be coupled to the motion of a magnetized mechanical resonator. Coherent manipulation of the spin is used to sense driven and Brownian motion of the resonator under ambient conditions with a precision below 6 picometers. With future improvements, this technique could be used to detect mechanical zero-point fluctuations, realize strong spin-phonon coupling at a single quantum level, and implement quantum spin transducers.

Hybrid quantum systems offer many potential applications in quantum information science and quantum metrology. One example is cavity quantum electrodynamics (cQED), in which a quantum two-level system (a qubit) is strongly coupled to resonant photons in an electromagnetic cavity (*1*–*3*). In the mechanical analog of cQED, the qubit is coupled to a mechanical resonator, with resonant phonons playing the role of cavity photons (*4*–*7*). Mechanical resonators are promising components for hybrid quantum systems because they couple to a wide range of forces while maintaining high quality factors (*8*–*13*) and can be fabricated using scalable techniques. A recent experiment demonstrated coupling of a superconducting phase qubit to the quantum motion of a piezoelectric resonator at millikelvin temperatures (*11*). However, this approach resulted in relatively short phonon lifetimes and is not easily extended to other resonator-qubit systems. An important goal is to extend this technique to nonpiezoelectric resonators that offer longer phonon lifetimes and to qubits featuring longer coherence times (*4*, *5*, *9*, *10*, *14*, *15*). In particular, spin states of localized atomlike systems in the solid state can be manipulated individually and can serve as an exceptional quantum memory, even under ambient conditions. Moreover, experiments have demonstrated that resonators can be sensitive to the magnetic force associated with a single electronic spin (*16*). Control over a coupled spin-resonator hybrid quantum system could be used to mediate long-range spin-spin coupling for quantum information applications (*17*) or to manipulate mechanical motion at the single quantum level with long qubit and phonon coherence times (*4*, *11*). In addition, coherent control over spin-phonon interactions is of direct relevance for realizations of novel nanoscale sensors (*18*–*20*).

In our experiment (Fig. 1A), we used the electronic spin associated with an individual nitrogen vacancy (NV) center to sense the motion of a nearby, magnetized atomic force microscopy (AFM) cantilever. The time-varying magnetic field generated by the displacement of the magnetic tip coherently drives the qubit evolution, which is subsequently detected via optical spin measurements. The essence of our approach (Fig. 1B) is to synchronize the evolution of the single spin with the cantilever's oscillations. When the spin is driven by a pulse train with a period matching the mechanical period, the motion constructively affects the spin evolution over a long interaction time, enhancing the spin's sensitivity in a narrow frequency band (*21*). In addition, the pulses dynamically decouple the NV spin from the slow evolution of the surrounding environment, increasing the possible interrogation time (*22*, *23*).

The NV centers are implanted ~5 nm below the surface of a bulk diamond sample. The spin sublevels $|m_s = 0\rangle$ and $|m_s = \pm 1\rangle$ of the electronic ground state exhibit a zero-field splitting of ~2.87 GHz. In the presence of a static magnetic field, the degeneracy between $|+1\rangle$ and $|-1\rangle$ is lifted, allowing us to selectively address the $|0\rangle \rightarrow |+1\rangle$ transition with microwave radiation. The magnetic field $\mathbf{B_{tip}}$ generated by the tip at the position of the NV results in an additional Zeeman shift of the splitting, given by $\Delta\omega = g_e \mu_B \mathbf{B_{tip}} \cdot \hat{\mathbf{z}} / \hbar$, where $g_e \approx 2$ is the electron g-factor, μ_B is the Bohr magneton, $\hbar$ is Planck's constant divided by 2π, and $\hat{\mathbf{z}}$ is the unit vector along the NV axis. With the tip held at a constant position, the static Zeeman shift is detected by performing continuous wave (CW) electron spin resonance (ESR) measurements (Fig. 1C). By scanning the tip at a fixed height above the diamond surface with a piezoelectric scanning stage and monitoring $\Delta\omega$, we mapped the projection of $\mathbf{B_{tip}}$ along the NV axis (Fig. 1D). This provides an accurate measurement of the magnetic field gradient G_m produced by the tip along the NV axis, which

[1]Department of Physics, Harvard University, Cambridge, MA 02138, USA. [2]Department of Physics, University of California Santa Barbara, Santa Barbara, CA, USA. [3]Institute for Quantum Optics and Quantum Information of the Austrian Academy of Science, 6020 Innsbruck, Austria. [4]Departments of Physics and Applied Physics, Yale University, New Haven, CT, USA.

*These authors contributed equally to this work.
†To whom correspondence should be addressed. E-mail: lukin@physics.harvard.edu

reaches up to 10^5 T/m; see supporting online material for further details (*24*).

The gradient G_m translates mechanical oscillations of the cantilever $x_{ac}(t)$ into an oscillating magnetic field $B_{tip,ac}(t) = G_m x_{ac}(t)$. Coherent control over the NV spin is used to measure $B_{tip,ac}$ via pulsed ESR techniques such as spin echo and longer dynamical decoupling sequences (*18*, *22*, *25*). To probe Brownian motion, which has a characteristic frequency but a randomly varying amplitude and phase, our measurement sequence cannot be phase-locked to the mechanical oscillation. For this reason, we measure the variance of the accumulated phase, yielding the mean square field amplitude $\langle B^2_{tip,ac} \rangle$. From $\langle B^2_{tip,ac} \rangle$ and G_m, the mean square motional amplitude $\langle x^2 \rangle$ can be inferred, which, for an undriven resonator, is related to the thermal occupation number $\bar{n}_{th} = \frac{k\langle x^2 \rangle}{\hbar \omega_r}$ (where k is the spring constant and ω_r is the mechanical resonance frequency).

In the measurement sequence used to detect $\langle x^2 \rangle$ (Fig. 2A), the NV's electronic spin is polarized in the $|0\rangle$ state via green illumination (*22*, *26*). Resonant microwaves tuned to the $|0\rangle \rightarrow |+1\rangle$ transition are applied to perform a Hahn echo sequence with free precession periods of length τ. The final $\pi/2$ pulse of the sequence converts the relative accumulated phase into a population difference that is read out via fluorescence (Fig. 2B) (*22*). With the cantilever drive switched off, the data (blue triangles) demonstrate collapses and revivals in spin coherence due to nearby carbon-13 (^{13}C) nuclear spins undergoing Larmor precession at the frequency $\omega_{nuc} = \gamma_{nuc} B_{dc}$, where $\gamma_{nuc}/2\pi = 1.07$ kHz/G is the gyromagnetic ratio of the ^{13}C nuclei and B_{dc} is the magnitude of the static magnetic field (*22*, *26*). The ensemble of ^{13}C nuclei produces an oscillating field with fluctuating amplitude and phase, resulting in collapses in coherence at odd multiples of π/ω_{nuc} and revivals at even multiples of π/ω_{nuc} (*22*). The tip is positioned relatively far from the NV, producing a weak gradient of $G_m = 100 \pm 12$ T/m, so in the absence of an external drive, the Brownian motion can be ignored and the field from the tip can be considered static. Red circles in Fig. 2B show the same measurement with the cantilever strongly driven. The evolution of the NV spin is dramatically affected by the cantilever motion. The revival is narrowed and shifted to $\tau = 2\pi/\omega_r$ due to $B_{tip,ac}$. Because the spin evolution is not phase-locked to the mechanical oscillation, $B_{tip,ac}$ has a constant amplitude but a uniformly distributed random initial phase ϕ_0 for each measurement, resulting in an echo signal given by a zero-order Bessel function (*24*). By fitting to this data, we determine the peak amplitude $B_{tip,ac} = 163 \pm 1$ mG and the oscillation frequency $\omega_r/2\pi = 80.14 \pm 0.07$ kHz, in agreement with the applied excitation frequency of 80.15 kHz. Incorporating the previously measured G_m, the root mean square (rms) amplitude of the tip motion, $x_{rms} = 114 \pm 14$ nm, can be extracted (*24*).

To measure the quality factor of the resonator (Fig. 2C), the resonator is driven to a fixed amplitude of motion, the drive is switched off, and we subsequently measure x_{rms} as a function of wait time after turning off the cantilever drive using the same protocol as in Fig. 2B. A quality factor of $Q = 211 \pm 6$ is extracted from the exponential decay of x_{rms}, in agreement with measurements made independently, using conventional interferometric readout of the cantilever motion, that yield $Q = 221 \pm 4$.

Under ambient conditions, the $\omega_r/2\pi = 80.15$ kHz resonator with $k \approx 3$ N/m has a thermal occupation number of $\bar{n}_{th} \approx 8 \times 10^7$ phonons, corresponding to Brownian motion with an rms amplitude of ~40 pm. To detect these oscillations with the single spin, we used a pulse sequence composed of N π-pulses known as XY4 (Fig. 3A) (*23*). This sequence further suppresses the effects of low-frequency magnetic noise and enhances the ac sensitivity by a factor of $\sim 1/(N^{3/2})$ in a narrow bandwidth (*21*, *23*). It also has the advantage of self-correcting pulse errors to first order for any accumulated phase of the NV spin (*23*).

We used an XY4 sequence with $N = 12$ π-pulses to measure resonator motion at excitation amplitudes of ~0, 57, 113, and 170 pm of rms-driven motion (Fig. 3B). Unlike the measurements

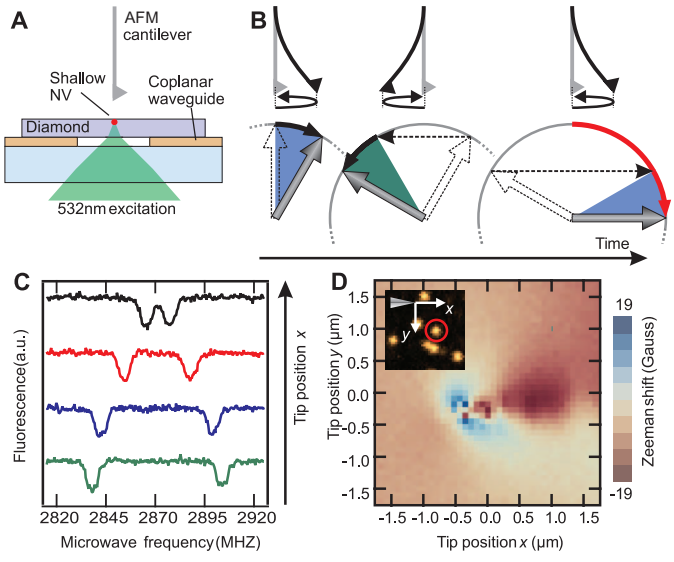

Fig. 1. Concept of the experiment. **(A)** A magnetized AFM cantilever tip is positioned within tens of nanometers of a shallow implant NV in bulk diamond. **(B)** The control pulse sequence is matched to the period of the mechanical resonator to constructively accumulate phase from the oscillations. Green and blue shaded regions show the accumulated phase of the spin during one half-period; horizontal dashed arrows show the effect of the microwave π-pulses. **(C)** CW-ESR spectra showing the transitions between the $|m_s = 0\rangle$ and $|m_s = \pm 1\rangle$ ground states of the NV as the tip is moved parallel to the axis of cantilever oscillations. A 12-G external magnetic field is applied opposite the static field from the tip. The four traces correspond to ~100-nm steps toward the NV. a.u., arbitrary units. **(D)** Scanning the tip at a fixed height above the surface, we extract a two-dimensional map of the dc field from the tip along the NV axis. Five pixels for which the shift could not be extracted were interpolated. (Inset) Fluorescence image of the diamond surface, with the NV used for this map circled in red.

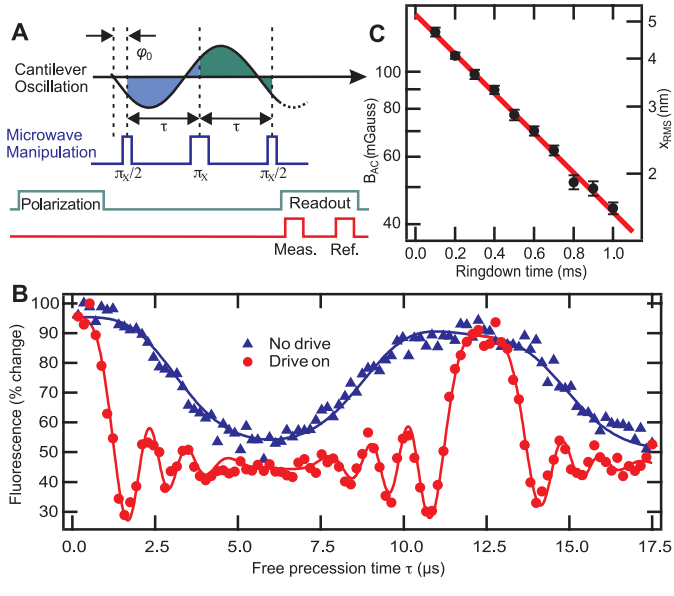

Fig. 2. Detection of driven motion **(A)** Hahn echo pulse sequence. The relative phase φ_0 varies for each measurement. **(B)** Spin-echo measurement with cantilever nearby with the drive switched off (blue triangles) and on (red circles). The Larmor precession of ^{13}C is tuned close to the mechanical frequency $\omega_r/2\pi = 80.15$ kHz via an external magnetic field of $B_{dc} \approx 78$ G. **(C)** Amplitude of ac magnetic field (left *y* axis) and motional amplitude (right *y* axis) as a function of wait time after switching off the drive, measured using spin echo. Here, $G_m = 2707 \pm 325$ T/m. Error bars correspond to the uncertainty in ac magnetic field (left *y* axis).

shown in Fig. 2, $B_{ext,dc}$ is tuned to a low value of ~10 G to extend the onset of the first collapse in spin coherence due to the ^{13}C nuclei's Larmor precession beyond the resonator-induced partial collapse (*24*). The multiple minima at 170 pm of rms-driven motion (green diamonds) are described by a Bessel function, as discussed above (*24*). Extracting x_{rms} from the fits in Fig. 3B and plotting against the ac driving voltage, the inclusion of Brownian motion is necessary to achieve good agreement with the data (Fig. 3C). The impact of Brownian motion on the spin is also directly evident in Fig. 3B in the slight dip in the undriven data (red circles) at $\tau = \pi/\omega_r = 6.2$ μs.

To further enhance the impact of Brownian motion on our NV spin, we used an XY4 sequence with $N = 16$ π-pulses, allowing the spin to accumulate more motion-induced phase in a single measurement (Fig. 3D). With the tip nearby at a gradient of 2940 ± 265 T/m, the Brownian motion induces a collapse in the NV spin coherence at $\tau = \pi/\omega_r$. The fits yield x_{rms} = 40 ± 5 pm and $\omega_r/2\pi$ = 79.7 ± 0.4 kHz, in agreement with the expected value of ~40 pm and the resonance frequency of 80.15 kHz. This corresponds to $B_{tip,ac} = 117 \pm 9$ nT rms. The tip's proximity to the NV affects the spin coherence, resulting in the offset between the two curves.

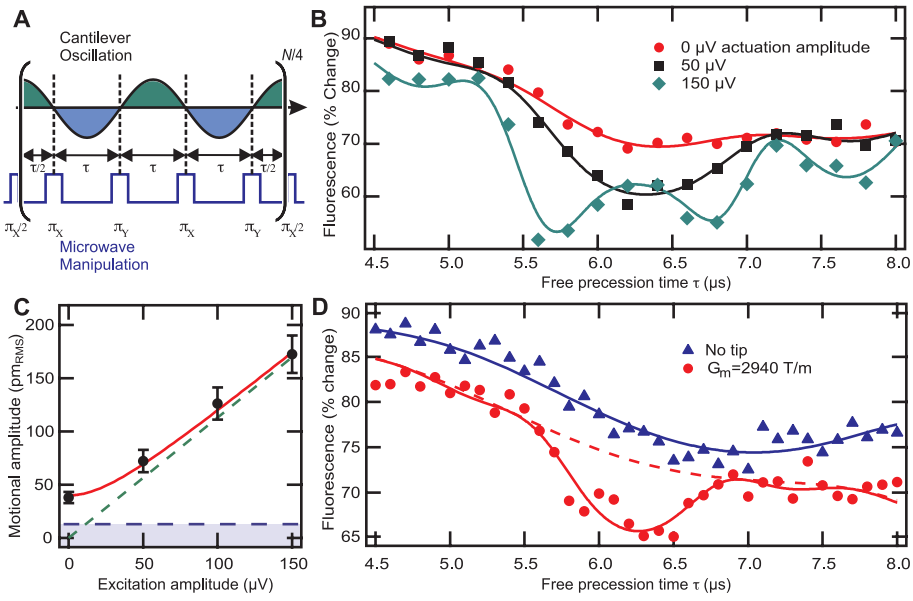

Fig. 3. Detection of Brownian motion. **(A)** XY4 pulse sequence. **(B)** XY4 measurement with $N = 12$ π-pulses for four different driving voltages (the 100-μV curve is excluded for clarity) at $G_m = 2978 \pm 268$ T/m. The fits account for Brownian and driven motion. **(C)** Extracted rms amplitude from (B) as a function of driving voltage. The red curve shows the expected rms amplitude based on independent calibrations, including thermal and driven motion, whereas the green dashed line is expected from driven motion alone. Neither line has any free parameters. The blue dashed line shows the estimated minimum detectable motion for the measurements in (B). Error bars indicate the statistical uncertainty in the fits and field-gradient measurements used to extract the motional amplitude. **(D)** XY4 measurement with $N = 16$ π-pulses, with the tip nearby at $G_m = 2940 \pm 265$ T/m (red circles) and without the tip (blue triangles). Solid lines are fits. The dashed red line shows the expected signal in the presence of a static tip with no Brownian motion.

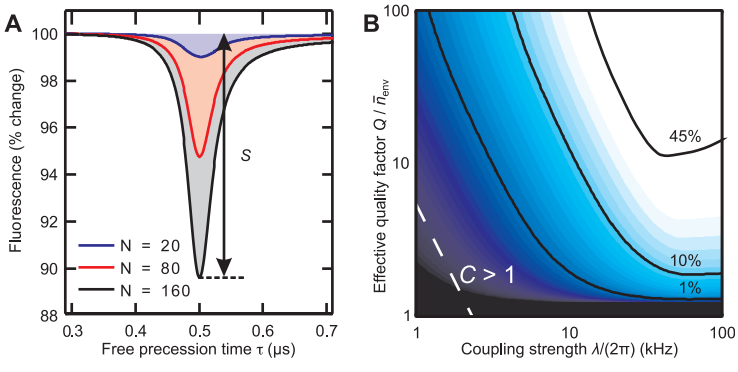

Fig. 4. Prospects for detection of zero-point motion. **(A)** Calculated XY4 signal for a cantilever cooled near its ground state, starting from an environmental temperature of $T_{env} = 4$ K. The signal S is the measurable impact from cantilever motion. Parameters are $\omega_r/2\pi = 1$ MHz, $\lambda/2\pi = 10$ kHz, $T_2 = 1$ ms, and $Q = 10^6$. **(B)** Signal S versus coupling strength and effective quality factor. The white dashed line marks the threshold of strong cooperativity, $C = \lambda^2 Q_{eff} \tilde{T}_2/\omega_r > 1$. At each point, we optimize the pulse number N within the experimental limitation of $N_{max} \leq 160$, as shown to be feasible in recent experiments (*21*, *23*). The slight upturn of the contours at large coupling is due to cantilever-induced decoherence (*24*); this small correction is neglected in Eq. 1.

Several recent experiments have reported that strongly driven mechanical resonators can influence the electronic spin of NV centers through the broadening and shifting of the spin transitions (*15*, *18*, *19*). Our approach takes advantage of the fact that the NV spin remains coherent for times much longer than the relatively short T_2^* (*26*). This longer interaction time enhances the spin's sensitivity to the resonator's motion (*22*, *25*) and enables the detection of picometer-scale oscillations without phase-locking.

To understand the present sensitivity limits and the potential for improvement, we consider a measurement of an undriven cantilever as in Fig. 3D. When the pulse sequence is synchronized with the cantilever such that $\tau = \pi/\omega_r$, the probability P_1 to find the spin in state $|1\rangle$ after the sequence is $P_1 = \frac{1}{2}[1 + e^{-N(\pi/\omega_r T_2)^3}] - S$, where we isolated the signal S due to the cantilever motion (*24*)

$$S \simeq \frac{1}{2} e^{-N(\pi/\omega_r T_2)^3} \left[1 - e^{-2N^2\lambda^2(2\bar{n}_{th}+1)W/\omega_r^2}\right] \quad (1)$$

Here, the coupling rate $\lambda = g_e \mu_B G_m a_0/\hbar$ is the Zeeman shift from a single phonon in the resonator, and $a_0 = \sqrt{\hbar/2m\omega_r}$ is the zero-point motion for a resonator of effective mass m. T_2 is the spin coherence time in the absence of the cantilever, whereas the exponent proportional to λ^2 describes the impact of the cantilever motion and depends on the mechanical Q, as well as the bandwidth of the control sequence through the factor $W = (1 + N/2Q)^{-1}$. The contribution from thermal motion is proportional to $\bar{n}_{th}$, and the remainder is due to quantum zero-point motion. Using Eq. 1 and including spin projection and shot noise through the single parameter K (*24*, *25*), we obtain the phonon number sensitivity $\eta = \bar{n}_{min}\sqrt{t_{tot}} = \frac{\sqrt{\pi}}{2KW\lambda^2} e^{N(\pi/\omega_r T_2)^3} \left(\frac{\omega_r}{N}\right)^{3/2}$, where $\bar{n}_{min}$ is the minimum detectable phonon occupation number in total measurement time t_{tot}. For the experimental parameters of Fig. 3D, we obtain $\eta \approx 2.5 \times 10^8$ phonons/$\sqrt{\text{Hz}}$, in agreement with the observed experimental sensitivity $\eta_{exp} \approx 4.9 \times 10^8$ phonons/$\sqrt{\text{Hz}}$ (*24*).

The main factor currently limiting our sensitivity is the coupling strength λ. Though we measure gradients up to 10^5 T/m, which gives $\lambda/2\pi \approx 8$ Hz, our most sensitive measurements are taken at ~3×10^3 T/m. The lower gradient is used because T_2 is found to decrease when the magnetic tip is very close to the NV; we observe a reduction of T_2 from ~160 μs when the tip is retracted to as low as ~5 μs when the tip is within 50 nm of the surface. Our use of XY4 dynamical decoupling sequences partially compensates for

this effect, indicating that the reduction in T_2 is due to low-frequency noise, which we attribute to magnetic domain noise of the tip material. We expect that this effect can be mitigated using alternative tip materials such as rare earth ferromagnets (*27*). The coupling strength can be further improved by using customized nanoresonators with a larger zero-point motion. Using state-of-the-art nanofabrication techniques, resonators with $Q > 10^6$, $\omega_r/2\pi \sim 1$ MHz (*28*), $G_m \sim 10^5$ T/m, and a coupling strength of $\lambda/2\pi \sim 10$ kHz can be fabricated (*4*), which, together with extended coherence times in isotopically purified diamond of $T_2 > 2$ ms (*29*) and faster pulse sequences with $N \sim 136$ pulses (*23*), yield a projected sensitivity of $\eta < 1$ phonon/$\sqrt{\text{Hz}}$. Combined with recently demonstrated single-shot spin readout (*30*), this raises the intriguing prospect of using a single NV center to sense mechanical motion at the scale of zero-point fluctuations in a single shot.

To assess the feasibility of sensing zero-point motion (Fig. 4A), we assume that the resonator is actively cooled near its motional ground state, using either the spin (*4*) or an additional system such as an optical or microwave cavity (*12*, *13*). Such cooling schemes are always accompanied by a decreased effective mechanical quality factor, $Q_{\text{eff}} = Q/\overline{n}_{\text{env}}$, where $\overline{n}_{\text{env}}$ is the phonon occupation number at the temperature of the surrounding environment. Inserting $\overline{n}_{\text{th}} = 0$ and $W = 2Q_{\text{eff}}/N$ into Eq. 1, a near maximal signal $S \sim 1/2$ is obtained, provided that $C = \lambda^2 Q_{\text{eff}} \tilde{T}_2/\omega_r > 1$, where $\tilde{T}_2 = T_2 N^{2/3}$ is the extended spin-coherence time due to dynamical decoupling (*23*). This is verified in Fig. 4B, which demonstrates that for a wide range of realistic parameters with $C > 1$, the zero-point motion of the resonator results in $S \sim 1/2$. The parameter C is a fundamental quantity in the physics of spin-phonon interactions. In direct analogy to the so-called cooperativity in cQED, $C > 1$ marks the onset of coherent quantum effects in a coupled spin-phonon system. Taking the optimized but realistic values $\lambda/2\pi = 10$ kHz, $T_2 = 1$ ms, $Q = 10^6$, $\omega_r/2\pi = 1$ MHz, and $N = 160$ pulses, we find that $C \sim 35$ can be reached at an environmental temperature of $T = 4$ K. Besides detection of zero-point motion, entering this regime could also enable coherent, long-range interactions between individual spins mediated by a mechanical resonator (*17*), which are of great interest for developing scalable, spin-based quantum information systems. Furthermore, by operating at lower environmental temperatures of $T \sim 100$ mK, it becomes possible to use the spin to cool the resonator down to its ground state (*4*) and to engineer quantum superpositions of mechanical motion, which could be read out using a coherent detection scheme like the one we present in this work.

The above considerations indicate that our approach provides an experimentally feasible route toward reaching strong coupling between single phonons and spins. Potential applications ranging from the creation and detection of quantum states of mechanical motion and the realization of quantum spin transducers to novel approaches for nanoscale sensing and readout (*19*, *20*) can be foreseen.

References and Notes

1. M. Scully, M. Zubairy, *Quantum Optics* (Cambridge Univ. Press, Cambridge, 1997).
2. S. Haroche, J. Raimond, *Exploring the Quantum: Atoms, Cavities, and Photons* (Oxford Univ. Press, New York, 2006).
3. R. J. Schoelkopf, S. M. Girvin, *Nature* **451**, 664 (2008).
4. P. Rabl *et al.*, *Phys. Rev. B* **79**, 041302 (2009).
5. P. Treutlein, D. Hunger, S. Camerer, T. W. Hänsch, J. Reichel, *Phys. Rev. Lett.* **99**, 140403 (2007).
6. F. Xue, L. Zhong, Y. Li, C. P. Sun, *Phys. Rev. B* **75**, 033407 (2007).
7. I. Bargatin, M. L. Roukes, *Phys. Rev. Lett.* **91**, 138302 (2003).
8. T. J. Kippenberg, K. J. Vahala, *Science* **321**, 1172 (2008).
9. G. A. Steele *et al.*, *Science* **325**, 1103 (2009).
10. D. Hunger *et al.*, *Phys. Rev. Lett.* **104**, 143002 (2010).
11. A. D. O'Connell *et al.*, *Nature* **464**, 697 (2010).
12. J. D. Teufel *et al.*, *Nature* **475**, 359 (2011).
13. J. Chan *et al.*, *Nature* **478**, 89 (2011).
14. M. D. LaHaye, J. Suh, P. M. Echternach, K. C. Schwab, M. L. Roukes, *Nature* **459**, 960 (2009).
15. O. Arcizet *et al.*, *Nat. Phys.* **7**, 879 (2011).
16. D. Rugar, R. Budakian, H. J. Mamin, B. W. Chui, *Nature* **430**, 329 (2004).
17. P. Rabl *et al.*, *Nat. Phys.* **6**, 602 (2010).
18. G. Balasubramanian *et al.*, *Nature* **455**, 648 (2008).
19. M. Grinolds *et al.*, *Nat. Phys.* **7**, 687 (2011).
20. C. Degen, *Appl. Phys. Lett.* **92**, 243111 (2008).
21. S. Kotler, N. Akerman, Y. Glickman, A. Keselman, R. Ozeri, *Nature* **473**, 61 (2011).
22. J. R. Maze *et al.*, *Nature* **455**, 644 (2008).
23. G. de Lange, Z. H. Wang, D. Ristè, V. V. Dobrovitski, R. Hanson, *Science* **330**, 60 (2010).
24. Materials and methods are available as supporting material on *Science* Online.
25. J. Taylor *et al.*, *Nat. Phys.* **4**, 810 (2008).
26. L. Childress *et al.*, *Science* **314**, 281 (2006).
27. B. C. Stipe, H. J. Mamin, T. D. Stowe, T. W. Kenny, D. Rugar, *Phys. Rev. Lett.* **86**, 2874 (2001).
28. S. S. Verbridge, H. G. Craighead, J. M. Parpia, *Appl. Phys. Lett.* **92**, 013112 (2008).
29. G. Balasubramanian *et al.*, *Nat. Mater.* **8**, 383 (2009).
30. L. Robledo *et al.*, *Nature* **477**, 574 (2011).

Acknowledgments: We thank T. Baart, M. Grinolds, P. Maletinsky, S. Hong, and A. Yacoby for stimulating discussions and R. Ilic, F. Koppens, and A. Zibrov for early contributions to the experiment. This work was supported in part by the NSF, the Center for Ultracold Atoms, the Air Force Office of Scientific Research Multidisciplinary University Research Initiative, the Defense Advanced Research Projects Agency Quantum-Assisted Sensing and Readout, the European Union (EU) Diamond-Based Atomic Nanotechnologies, and the Packard Foundation. S.K. acknowledges support by the U.S. Department of Defense through the National Defense Science and Engineering Graduate Program and the NSF through the Graduate Research Fellowship Program under grant no. DGE-1144152. Q.U. acknowledges support from Deutschen Forschungsgemeinschaft, and P.R. acknowledges support by the EU network Atomic Quantum Technologies Integrating Project and the Austrian Science Fund (FWF) through Sonderforschungsbereich FOQUS and the START grant Y 591-N16.

Supporting Online Material

www.sciencemag.org/cgi/content/full/science.1216821/DC1
Materials and Methods
SOM Text
Figs. S1 to S3
Tables S1 and S2
References

18 November 2011; accepted 8 February 2012
Published online 23 February 2012;
10.1126/science.1216821

Hydrocarbon Separations in a Metal-Organic Framework with Open Iron(II) Coordination Sites

Eric D. Bloch,[1] Wendy L. Queen,[1,2] Rajamani Krishna,[3] Joseph M. Zadrozny,[1] Craig M. Brown,[2,4] Jeffrey R. Long[1,5]*

The energy costs associated with large-scale industrial separation of light hydrocarbons by cryogenic distillation could potentially be lowered through development of selective solid adsorbents that operate at higher temperatures. Here, the metal-organic framework $Fe_2(dobdc)$ ($dobdc^{4-}$: 2,5-dioxido-1,4-benzenedicarboxylate) is demonstrated to exhibit excellent performance characteristics for separation of ethylene/ethane and propylene/propane mixtures at 318 kelvin. Breakthrough data obtained for these mixtures provide experimental validation of simulations, which in turn predict high selectivities and capacities of this material for the fractionation of methane/ethane/ethylene/acetylene mixtures, removal of acetylene impurities from ethylene, and membrane-based olefin/paraffin separations. Neutron powder diffraction data confirm a side-on coordination of acetylene, ethylene, and propylene at the iron(II) centers, while also providing solid-state structural characterization of the much weaker interactions of ethane and propane with the metal.

As a consequence of the similar sizes and volatilities of the molecules, separations of olefin/paraffin mixtures, such as ethylene/ethane and propylene/propane, must currently be performed at low temperatures and high pressures and are among the most energy-intensive separations carried out at large scale in the chemical industry (*1*). Because these gas mixtures are produced by cracking long-chain hydrocarbons at elevated temperatures, a substantial energy penalty arises from cooling the gases to the low temperatures required for distillation. Thus, tremendous energy savings could be realized if materials enabling the efficient separation of olefins and paraffins at higher temperatures (than currently used in distillation) and atmo-